One-step approach for the synthesis of $CoFe_2O_4$@rGO core-shell nanocomposites as efficient adsorbent for removal of organic pollutants

Z. J. Song, W. Ran and F. Y. Wei

ABSTRACT

$CoFe_2O_4$-reduced graphene oxide nanocomposites (CFG) have been successfully synthesized via one-step solvothermal method. The prepared CFG are characterized by X-ray diffraction, Raman spectroscopy, Fourier transform infrared spectroscopy, field emission scanning electron microscopy (FESEM), vibrating sample magnetometer and so on. The FESEM results show that CFG have uniform core-shell structure with an average diameter of about 75 nm and the thickness of the outer graphene shell is about 15–20 nm. The mass ratio of $CoFe_2O_4$ to graphene oxide is a key factor affecting the formation of core-shell hybrids. CFG display much higher adsorption capacity for anionic dyes than cationic dyes owing to the favorable electrostatic interaction. The adsorption capacity for methyl orange is observed as high as 263 mg g^{-1} at 298 K, and the adsorption isotherms follow the Langmuir model. Furthermore, the specific saturation magnetization (Ms) of CFG is 32.8 emu g^{-1}, and the as-synthesized nanocomposites can be easily separated by external magnetic field after adsorption. The results suggest that CFG have great potential for the practical industrial wastewater treatment.

Key words | anionic dyes, $CoFe_2O_4$-reduced graphene oxide nanocomposites, core-shell structure, one-step method, selective adsorption

Z. J. Song
W. Ran
F. Y. Wei (corresponding author)
School of Chemistry and Chemical Engineering,
Hefei University of Technology,
Tunxi Road 193,
Hefei 230009,
China
E-mail: *weifyliuj@hfut.edu.cn*

INTRODUCTION

In recent years, graphene/magnetic oxide (GM) nanocomposites have drawn tremendous scientific interest for their distinguished properties such as strong superparamagnetism, large surface area and excellent extraction ability. GM composites have been successfully applied in drug carriers (Yang *et al.* 2009), catalyst (Fu *et al.* 2012; Yao *et al.* 2013), lithium storage (Yang *et al.* 2010; Sun *et al.* 2014) and other fields (Liu *et al.* 2013; Xue *et al.* 2014). In addition, GM composites are excellent adsorbents in the field of water treatment. Until now, the adsorptive removal of dyes and heavy metal ions by this type of nanocomposites has been demonstrated. Li *et al.* (2011) synthesized magnetic $CoFe_2O_4$-functionalized graphene sheets (FGS) nanocomposites by hydrothermal treatment, and discovered that the cobalt ferrite nanoparticles with diameters of 10–40 nm were uniformly distributed on FGS, and the adsorption capacity for removing methyl orange (MO) is 71.54 mg.g^{-1}. Qi *et al.* (2015) found that magnetite/reduced graphene oxide (MRGO) nanocomposites obtained by different methods have different characteristics. The MRGO prepared by the co-precipitation method showed special adsorption ability to negative ions, but those synthesized by the solvothermal method had the best extraction ability and reusability to metal ions. Nevertheless, these reported magnetic nanoparticles are loaded on the surface of graphene sheets (Xie *et al.* 2012; Li *et al.* 2014), and may have the defects of detachment and aggregation of magnetic metal oxides from graphene sheets, which decreased their saturation magnetization (Fu *et al.* 2013; Zhan *et al.* 2015), and reduced their efficacy in practical applications. One of the most promising strategies to tackle the aggregation problem of metal oxides is to enwrap them with a polymer or silica shell (Dong *et al.* 2006; Luo *et al.* 2009). However, the reported materials enwrapped with the polymer or silica shell showed low saturation magnetization. Therefore, the fabrication of core-shell magnetic nanocomposites with both strong magnetic responsivity and high absorption capacity remains challenging. Core-shell structure Fe_3O_4@graphene oxide (GO) submicron particles have

doi: 10.2166/wst.2016.520

been prepared via the two-step electrostatic self-assembly process and exhibited large adsorption capacity for bovine serum albumin (BSA) (Wei *et al.* 2012).

In this paper, we develop a simple solvothermal route to prepare the core-shell structure $CoFe_2O_4$@rGO (abbreviated as CFG) nanocomposites, in which the reduction of GO and the crystallization of $CoFe_2O_4$ crystals happened in one step without adding any reducing agent. The formation mechanism of the core-shell structure was initially discussed. The adsorption properties were also measured using MO as model pollutant in aqueous solutions. The core-shell nanocomposites can suppress the aggregation of oxide nanoparticles, maintain a high saturation magnetization and give rise to a high adsorption capacity. The obtained CFG can be recyclable, and thus has great potential for the removal of toxic pollutants from wastewater.

EXPERIMENTS

Materials

Graphite powder, ethylene glycol (EG), polyethylene glycol 2000 (PEG 2000), anhydrous ferric chloride ($FeCl_3$), cobalt (II) chloride hexahydrate ($CoCl_2{\cdot}6H_2O$), methylene blue (MB), MO, Congo red (CR), Rhodamine B (RhB) and other reagents were purchased from Sinopharm Chemical Reagent Co. (Hefei, China). All chemicals used here are analytical grade without further purification.

Preparation of CFG

GO was synthesized by the modified Hummers method (Marcano *et al.* 2010). CFG were prepared by solvothermal method with minor modifications (Xue *et al.* 2014). In a typical synthesis, the as-prepared GO (0.291 g) was exfoliated by ultrasonication in 70 mL of EG and 2.5 g of polyethylene 2000 (PEG 2000) mixture at 75 °C, followed by the addition of $FeCl_3$ (2 g) and $CoCl_2{\cdot}6H_2O$ (1.42 g) to form a brown mixture solution. 30 mL of EG solution containing 9 g of NaAc and 1 g of NaOH were slowly added into the above brown solution, followed by vigorous stirring for 2 h. The whole process was kept ultrasonic to avoid the aggregation of the GO in EG. After that, the resulting mixture was sealed in a Teflon-lined stainless-steel autoclave, maintained at 453 K for 24 h, then cooled naturally to room temperature. The black products were obtained by magnetic separation, washed several times with absolute ethanol and deionized water and dried at 333 K for 12 h.

Characterization

The powder X-ray diffraction (XRD) patterns of the samples were performed using a Rigaku D/max 2500 V X-ray diffractometer with CuKα radiation (λ = 1.5418 Å). The morphology and structure of the samples were characterized by a field emission scanning electron microscope (FESEM, Hitachi SU8020) and high-resolution transmission electron microscope (HRTEM, JEM-2100F). Fourier transform infrared spectroscopy (FTIR) spectra were recorded on a Perkin-Elmer Spectrum 100. X-ray photoelectron spectroscopy (XPS) was conducted using an ESCALAB 250 spectrometer. The magnetic properties of samples were studied using a vibrating sample magnetometer (VSM, PPMS-14T) at a temperature of 300 K. The zeta potential was measured by the ZETASIZER Nano-ZS from Malvern Instruments.

Adsorption experiments

The adsorption of dyes in aqueous solution on CFG was performed in a batch experiment. Typically, 0.025 g of the adsorbent was added into 25 mL of MO solutions of the desired initial concentrations (10 mg L^{-1}) and then the mixture was shaken at a speed of 180 rpm at 298 K for 2 h. The nanocomposites were removed from the solution by magnetic separation, and the concentrations of MO, CR, MB, and RhB were determined by a Vis spectrophotometer (722, China) at 465, 497, 662 and 550 nm, respectively. The adsorption capacity q_e and removal efficiency R were calculated by the following expressions:

$$q_e = \frac{(C_0 - C_e)V}{m} \tag{1}$$

$$R = \frac{(C_0 - C_e)}{C_0} \times 100\% \tag{2}$$

where q_e (mg g^{-1}) represents the adsorption capacity at equilibrium, C_0 and C_e (mg L^{-1}) are the initial and the equilibrium concentration of the dye remaining in the solution. V (L) is the volume of the aqueous solution, and m (g) is the dry weight of composites.

Reusability experiment

CFG (0.1 g) was added to 50 mL of MO solution (100 mg L^{-1}) and then the mixture was shaken for 1.5 h at room temperature. After separation of the nanocomposites by an external

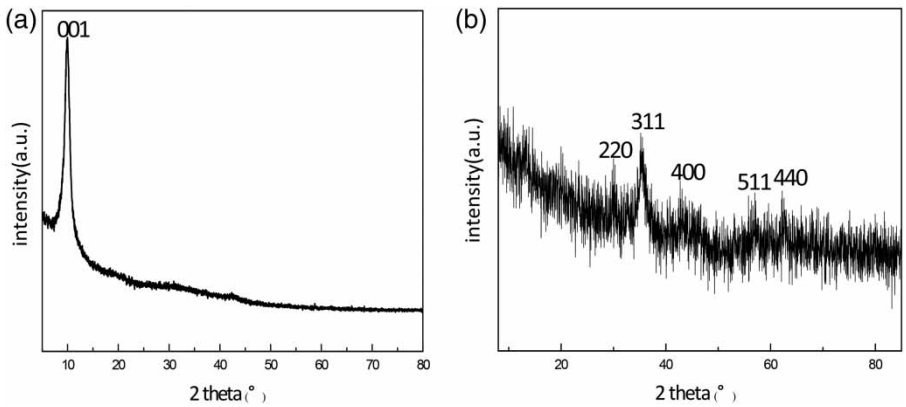

Figure 1 | XRD patterns of (a) GO and (b) CFG.

magnet, the supernatant solution was analyzed. The nanocomposites' adsorbent with MO was washed with absolute ethanol solution several times, collected by a magnet and reused for the next adsorption experiment. The reusability experiments were performed six times.

RESULTS AND DISCUSSION

Structure and morphology of samples

The phase structures of as-synthesized samples were firstly determined by XRD. As shown in Figure 1(a), the GO shows a sharp peak at $2\theta = 9.4^\circ$ corresponding to the (001) reflection of GO. By contrast, the characteristic peak of GO cannot be detected in the XRD pattern of the CFG (Figure 1(b)), suggesting that GO was effectively reduced (Yao *et al.* 2012b). Meanwhile, the main diffraction peaks at $2\theta = 30.1$, 35.3, 42.7, 56.8 and 62.2° match well with the cubic spinel structure of cobalt ferrite (JCPDS card no. 22-1086), and correspond to crystal indexes of (220), (311), (400), (511), and (440), respectively (Wan & Jian 2015).

Figure 2 shows a comparison of Raman spectra of $CoFe_2O_4$ and CFG, recorded in the frequency range 100–2,200 cm^{-1}. For all the samples, three major Raman active modes of broadening peaks are detected clearly at about 298, 456, and 666 cm^{-1}, which shows that the prepared nanocomposites consisted of $CoFe_2O_4$ (Ding *et al.* 2015). In comparison with the $CoFe_2O_4$, CFG shows a Raman shift around 1,352 and 1,593 cm^{-1} corresponding to the D band and G band of grapheme oxide (Gan & Shang 2015). The existence of these two bands in CFG shows that the graphene has been incorporated into the nanoparticle system (An *et al.* 2014). Meanwhile, the ratio of intensities (I_D/I_G)

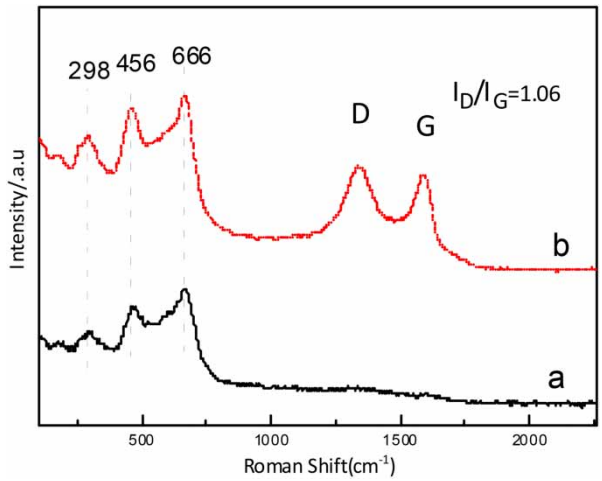

Figure 2 | Raman spectra of (a) $CoFe_2O_4$, (b) CFG.

represents the structure defect degree of the graphite materials. The value of I_D/I_G for GO was 0.93. For CFG, that was markedly increased to 1.06, indicating formation of some sp^3 carbon by functionalization as a large number of oxygen groups were removed in the solvothermal reduction process (Joon *et al.* 2012).

FTIR spectra of GO, $CoFe_2O_4$, and CFG are shown in Figure 3. Several characteristic peaks of GO can be observed in Figure 3(a), confirming the successful oxidation of graphite. In detail, the intense band at 3,423 cm^{-1} originated from O–H stretching vibration. The bands at 1,735 and 1,620 cm^{-1} are associated with C=O stretching of COOH groups located at edges of GO sheets. The bands at 1,196 and 1,050 cm^{-1} are attributed to the stretching of epoxy C–O and alkoxy C–O band (Xie *et al.* 2012), respectively. By comparison, most bands related to the oxidized groups vanish in the FTIR (Figure 3(c)) of CFG except for two weak peaks at 3,423 cm^{-1} (υ (O–H)) and 1,082 cm^{-1}

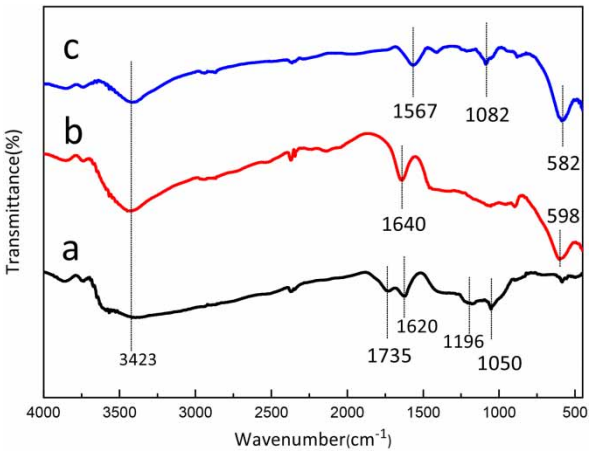

Figure 3 | FTIR spectra of (a) GO, (b) $CoFe_2O_4$, and (c) CFG.

(υ (C–O)), revealing that GO was effectively reduced in the synthesis process. For $CoFe_2O_4$ (Figure 3(b)), the peak at around 598 cm^{-1} was observed, which is assigned to the Fe(Co)–O band in the cobalt ferrite (Lu *et al.* 2014). The absorption peak at 1,640 cm^{-1} is ascribed to the vibration of adsorbed water (Zhang *et al.* 2015). The new adsorption band at 1,567 cm^{-1} in FTIR of CFG can be assigned to the stretching vibrations of the un-oxidized carbon backbone (Ji *et al.* 2011). Meanwhile, the stretching vibration of Fe(Co)–O band at 598 cm^{-1} gets red shift to 582 cm^{-1}.

To investigate the morphology and particle size of the products, Figure 4 gives the corresponding FESEM and HRTEM images. The FESEM image of GO (Figure 4(a)) displays a wrinkled and scrolled morphology paper-like structure of the ultrathin graphene sheets and stacking of sheets. For the $CoFe_2O_4$ nanoparticles (Figure 4(b)), uniform spheres with an average diameter of approximately 120 nm are observed. It is found that their diameters are mainly distributed in the range of 80–160 nm (Figure 5(a)). From Figure 4(c), CFG becomes smaller with an average diameter of about 75 nm, the diameter distribution being in the range of 50–105 nm (Figure 5(b)). Furthermore, compared with $CoFe_2O_4$ nanoparticles, CFG becomes more irregular. It may contribute to retarding the crystalline rate of $CoFe_2O_4$ by the graphene sheets during the solvothermal process. The HRTEM image of the CFG (Figure 4(d))

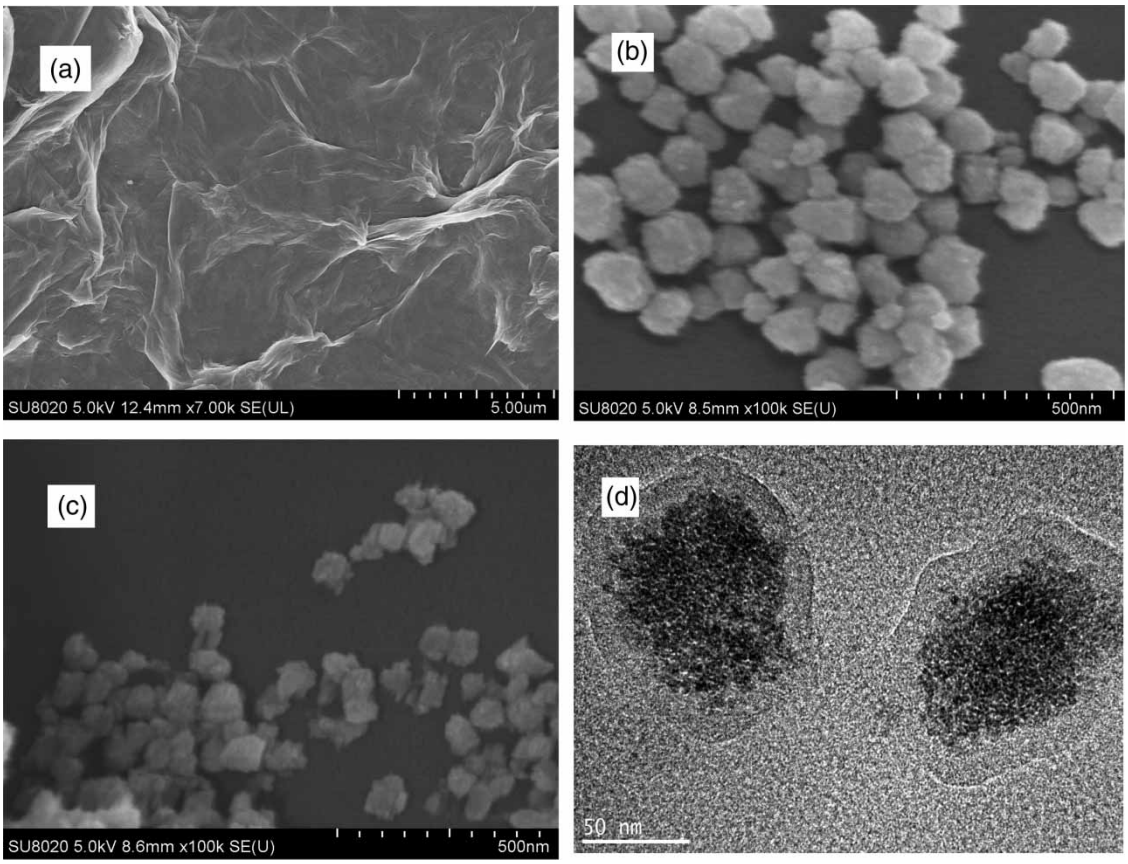

Figure 4 | FESEM images of (a) GO, (b) $CoFe_2O_4$, (c) CFG, and (d) HRTEM image of CFG.

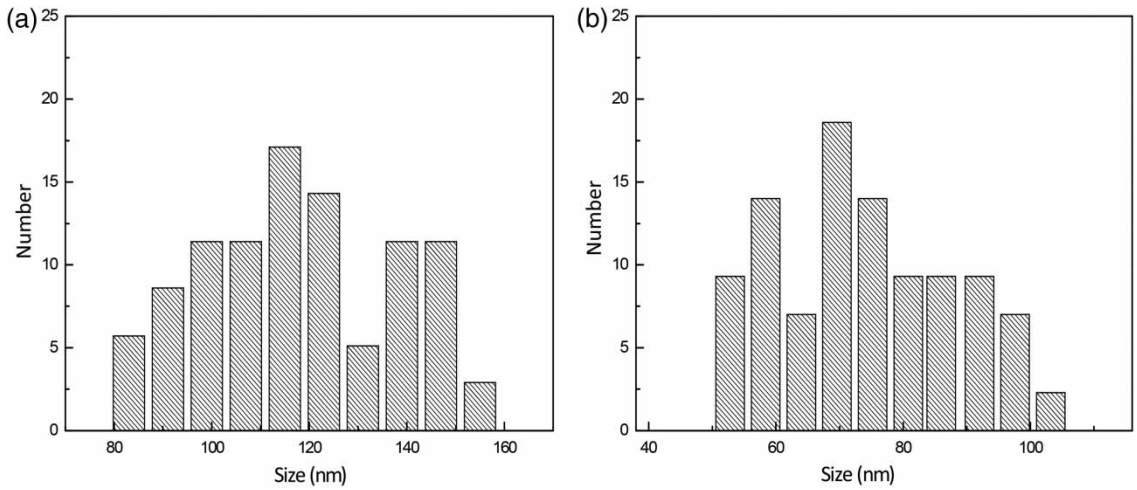

Figure 5 | The diameter distribution of (a) $CoFe_2O_4$ and (b) CFG.

indicates that the $CoFe_2O_4$ nanoparticles are coated with a uniform shell of graphene with the thickness of approximately 15–20 nm and the diameter of the $CoFe_2O_4$ core is around 50 nm. This means that a novel type of core-shell structure CFG has been successfully synthesized.

In the present work, it is worth noting that the magnetic $CoFe_2O_4$ nanoparticles decorated onto graphene sheets are obtained under the same conditions only by decreasing the mass ratio of $CoFe_2O_4$ to GO to 3. According to previous reports (Sharifi *et al.* 2013), there are several factors that may contribute to the formation of the core-shell CFG. First, the existence of the van der Waals forces between the adjacent magnetic $CoFe_2O_4$ nanoparticles make them move towards each other and GO sheets are aggregated simultaneously. Second, the graphene sheet can roll itself up into a scroll structure under ultrasonic effect. Third, the nanoparticles attached at the edge of the GO sheets may be attracted by the inner part of the GO sheets due to sparsely distributed oxygen-containing functional groups preceding the rolling (Xue *et al.* 2014). Although the detailed mechanism of the growth of graphene-$CoFe_2O_4$ core-shell nanocomposites is not very clear, it is obvious that the mass ratio of $CoFe_2O_4$ to GO is a key factor for the formation of core-shell hybrids.

Vibrating sample magnetometer analysis

To evaluate the magnetic separation capacity of CFG, we conducted the magnetic hysteresis loops of CFG and pure $CoFe_2O_4$ at 300 K, as shown in Figure 6. The saturation magnetization (Ms) of the pure $CoFe_2O_4$ nanoparticles is 45.4 emu g^{-1}, whereas the Ms value of CFG is 32.8 emu g^{-1},

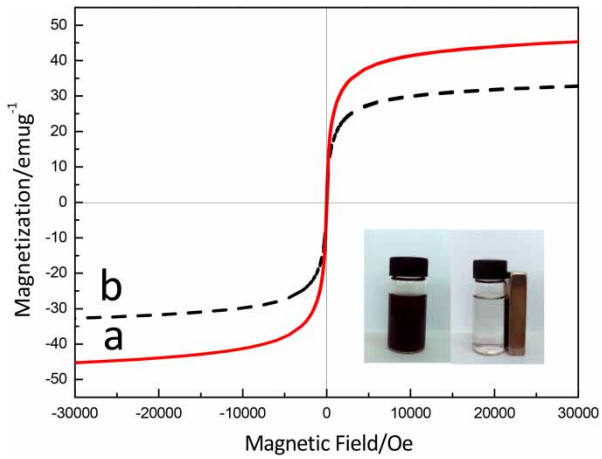

Figure 6 | VSM magnetization curves of (a) $CoFe_2O_4$ and (b) CFG. The inset shows the separation of CFG from aqueous solution under an external magnetic field.

which is slightly lower than that of pure $CoFe_2O_4$, but much higher than that of the magnetic metal oxides-graphene sheets hybrid composites (Li *et al.* 2011; Xie *et al.* 2012). The HRTEM image shows that CFG possesses a magnetically inactive shell of graphene, thus affecting the magnitude of magnetization. The magnetic separability of CFG was also tested by placing a magnet near the glass bottle. The black product was rapidly attracted toward the magnet in a short period (inset in Figure 6), demonstrating high magnetic sensitivity of CFG.

Removal of dyes from aqueous solution

The adsorption performances of four organic dyes (two cationic dyes and two anionic dyes) on CFG were also studied.

The adsorption isotherms at room temperature are shown in Figure 7. The data of maximum adsorption for these dyes are summarized in Table 1. The results show that CFG have stronger affinity for anionic dyes than for cationic dyes.

Zeta potential of adsorbent is a key factor to influence its adsorption capacity, and thus is measured to understand further why CFG can remove anionic dye more effectively than cationic dye. The zeta potential value of CFG synthesized using EG as solvent is about 30.3 mV, indicating that the surface of CFG is positively charged. The high absolute zeta potential value also proves that the adsorbent will be stable in aqueous solution (Fan *et al.* 2013; Qi *et al.* 2015). In addition, we find that the zeta potential value of CFG synthesized with EG/H_2O mixed solution as solvent will drop to –25.3 mV, and thus the adsorption capacity for anionic dyes is obviously decreased.

Based on the above, the mechanism of the adsorption of organic dyes by CFG is probably due to electrostatic interaction. For instance, MO is an anionic azo dye which contains the sulfonic acid groups (R-SO_3Na). In aqueous solution, dye dissociates to the sulfonate anions (R-SO_3^-) and the sodium ions (Na^+). Therefore, R-SO_3^- ions were easily absorbed to the surface of CFG by electrostatic force. Although the detailed formation mechanism of CFG surface charge was not very clear, it is certain that the type of reaction media caused some surface modifications onto CFG owing to the difference in the surface tension and dielectric constant (Ramesha *et al.* 2011; Hayyan *et al.* 2015).

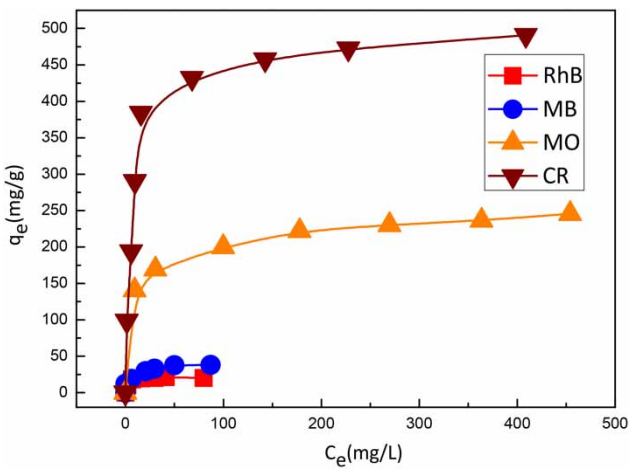

Figure 7 | Adsorption isotherms of dyes on CFG.

Table 1 | The maximum adsorption capacities q_{max} of different dyes on CFG

	Dye	q_{max} (mg.g^{-1})
Anionic	MO	246
	CR	491
Cationic	MB	38
	RhB	21.5

Desorption and reuse of adsorbents

The recycling and regeneration ability is significant for the practical application of adsorbents. Therefore, the recycling of CFG in the removal of MO was investigated. Figure 8 shows the removal efficiency of MO on CFG as a function of cycling runs. The values of R after 1.5 h are 98.5, 96.1, 93.8, 92.2, 90.3 and 88.6% for the consecutive six cycles, respectively. The decline of removal efficiencies is not

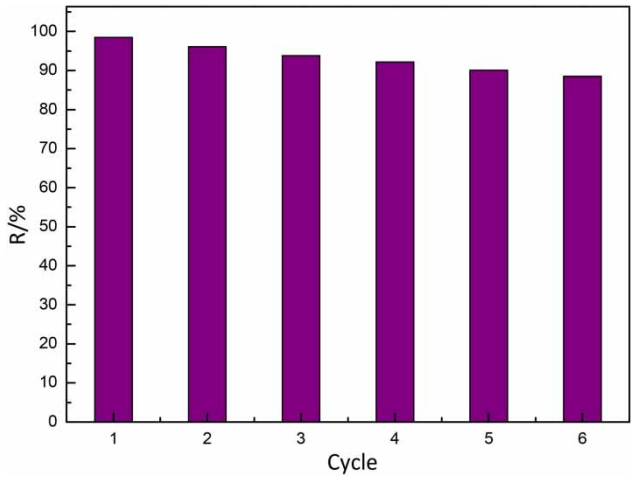

Figure 8 | The relationship of the removal efficiency of MO on CFG with cycles.

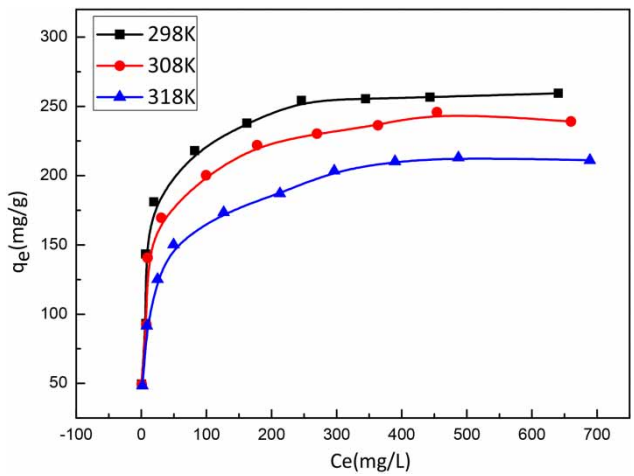

Figure 9 | Adsorption isotherms of MO on CFG.

Table 2 | Parameters for Langmuir and Freundlich isotherm models

	Langmuir model				Freundlich model			
T (K)	q_{max} (mg g^{-1})	b (L mg^{-1})	R^2	F	K_F (mg$^{(1-n-1)}$L^n·g^{-1})	n	R^2	F
298	263	0.09	0.9996	17,374	119	7.68	0.95293	143
308	246	0.07	0.99873	5,515	107	7.46	0.9709	234
318	220	0.04	0.99865	5,181	77	6.1	0.95922	165

more than 10% after six recycles, indicating that CFG have a good reusability.

Adsorption isotherms analysis of MO

The adsorption isotherms of MO on CFG are shown in Figure 9 at 298, 308 and 318 K. The Langmuir isotherm model (Yao *et al.* 2012a, 2012b) is used to describe the monolayer adsorption process, and the model can be described in linear form by the following equation:

$$\frac{c_e}{q_e} = \frac{1}{q_{\max} b} + \frac{1}{q_{\max}} c_e \tag{3}$$

where q_{max} (mg g^{-1}) is the maximum adsorption capacity at complete monolayer coverage, b (L mg^{-1}) is the Langmuir adsorption constant.

The Freundlich isotherm model (Sharifi *et al.* 2013) shows that the multilayer of the adsorption process occurs on heterogeneous surfaces, and is expressed as follows:

$$\ln q_e = \ln K_F + \frac{1}{\mathrm{n}} \ln c_e \tag{4}$$

where K_F ((mg^{1-n}L^n)·g^{-1}) represents the adsorption capacity, and n represents the degree of dependence of adsorption with equilibrium concentration.

The related parameters of two models are calculated and displayed in Table 2. From the linear correlation coefficients (R^2) at different temperatures, it can be found that the Langmuir model is more suitable for describing the adsorption of MO on CFG compared to the Freundlich model. In addition, the F values obtained from the Langmuir equation are far higher than those from the Freundlich equation. The results suggest that monolayer adsorption of MO on CFG is the main mechanism (Li *et al.* 2012). Besides, the values of q_{max} calculated from the Langmuir model are the highest at T = 298 K and the lowest at T = 318 K, which indicates that increasing temperature is unfavorable to the adsorption and the adsorption process is exothermic.

Calculated from the Langmuir isotherm model, the maximum equilibrium adsorption capacity (q_{max}) of MO on CFG is 263 mg g^{-1} at 298 K. A comparison of q_{max} for MO uptake between CFG and different magnetic adsorbents reported in the literature can be seen in Table 3. It is obvious that CFG synthesized in this work exhibits quite a high q_{max}, which suggests that the as-synthesized CFG can be considered as an effective adsorbent for the removal of MO dye from wastewater.

Adsorption thermodynamics

Thermodynamics parameters including Gibbs free energy change (ΔG), enthalpy change (ΔH), and entropy change (ΔS) are calculated from the adsorption isotherms (Figure 9). ΔG is calculated using Equation (5). ΔH and ΔS are determined from the slope and intercept of the plot of $\ln K_0$ versus $1/T$ using Equation (6):

$$\Delta G = -RT \ln K_0 \tag{5}$$

Table 3 | Summary of MO maximum adsorption capacities on various magnetic adsorbents

	Adsorption capacity		
Adsorbent	q_{max} (mg.g^{-1})	T/K	Reference
$ZnLa_{0.02}Fe_{1.98}O_4$/MWCNTs	81	298	Zhang & Nan (2015)
Co/MWCNTs	170	293	Zhao *et al.* (2015)
MPGM	80	298	Wang *et al.* (2015)
MWCNT/SPIONs	10.89	298	Bayazit (2014)
$CoFe_2O_4$–FGS	71.54	300	Li *et al.* (2011)
m-CS/g-Fe_2O_3/MWCNTs	66	293	Shuang *et al.* (2012)
CFG	263	298	This work

Table 4 | Values of thermodynamic parameters for MO adsorption on CFG

T(K)	ΔG (kJ mol^{-1})	ΔH (kJ mol^{-1})	ΔS (J mol^{-1} K^{-1})
298	–47.3	–34.8	41.9
308	–46.4		37.7
318	–39.7		15.4

$$\ln K_0 = \frac{\Delta S}{R} - \frac{\Delta H}{RT} \quad (6)$$

where R and T represent the universal gas constant (8.314 J mol^{-1} K^{-1}) and the system temperature (K). K_0 is the equilibrium distribution coefficient that is obtained by plotting $\ln(q_e/C_e)$ versus q_e and extrapolating q_e to zero.

The thermodynamic data calculated by Equations (5) and (6) are shown in Table 4. The value of ΔH during the adsorption process is calculated to be –34.8 kJ mol^{-1}, which indicates that the adsorption process is exothermic. Meanwhile, the ΔS values are all positive at different temperatures, which illustrate the increasing randomness at the solid-solution interface during fixation of MO onto the surface of CFG. The negative values of ΔG demonstrate a spontaneous and feasible process for the adsorption. The value of ΔG becomes more negative with the decrease of temperature, which indicates that the adsorption is suitable at low temperature.

CONCLUSIONS

In summary, we have synthesized a novel type of core-shell structure $CoFe_2O_4$@rGO nanocomposites (CFG) via a facile one-step solvothermal route. The as-synthesized CFG have a uniform core-shell structure with an average diameter of about 75 nm, where the $CoFe_2O_4$ nanoparticles are coated by a layer shell of GO with a thickness of approximately 15–20 nm. The mass ratio of $CoFe_2O_4$ to GO is a key factor for the formation of core-shell hybrids. CFG displays much higher adsorption capacity for anionic dyes owing to electrostatic interaction between CFG and dyes. Compared with previous literature, CFG exhibits a very high absorption capacity of 263 mg g^{-1} for MO at 298 K, and the prepared CFG nanocomposites can be easily separated by an external magnetic field after adsorption. After six cycles of the adsorption–desorption process, their adsorption capacity decreased slightly. This work indicates that CFG have great potential for organic pollutants wastewater treatment.

ACKNOWLEDGEMENTS

This work was supported by the National Natural Science Foundation of China (No. 51372062).

REFERENCES

An, S., Joshi, B. N., Min, W. L., Na, Y. K. & Yoon, S. S. 2014 Electrospun graphene-ZnO nanofiber mats for photocatalysis applications. *Appl. Surf. Sci.* **294** (5), 24–28.

Bayazit, Ş. S. 2014 Magnetic multi-wall carbon nanotubes for methyl orange removal from aqueous solutions: equilibrium, kinetic and thermodynamic studies. *Sep. Sci. Technol.* **49** (9), 1389–1400.

Ding, Z., Wang, W., Zhang, Y. J., Li, F. & Liu, J. P. 2015 Synthesis, characterization and adsorption capability for Congo red of $CoFe_2O_4$ ferrite nanoparticles. *J. Alloy Compd.* **640**, 362–370.

Dong, K. Y., Su, S. L., Papaefthymiou, G. C. & Ying, J. Y. 2006 Nanoparticle architectures templated by SiO_2/Fe_2O_3 nanocomposites. *Chem. Mater.* **18** (3), 614–619.

Fan, X. J., Jiao, G. Z., Zhao, W., Jin, P. F. & Li, X. 2013 Magnetic Fe_3O_4-graphene composites as targeted drug nanocarriers for pH-activated release. *Nanoscale* **5** (3), 1143–1152.

Fu, Y. S., Chen, H. Q., Sun, X. Q. & Wang, X. 2012 Combination of cobalt ferrite and graphene: High-performance and recyclable visible-light photocatalysis. *Appl. Catal. B* **111–112**, 280–287.

Fu, M., Jiao, Q. Z. & Zhao, Y. 2013 Preparation of $NiFe_2O_4$ nanorod-graphene composites via an ionic liquid assisted one-step hydrothermal approach and their microwave absorbing properties. *J. Mater. Chem. A* **1** (18), 5577–5586.

Gan, L. & Shang, S. M. 2015 Covalently functionalized graphene with D-glucose and its reinforcement to poly(vinyl alcohol) and poly(methyl methacrylate). *RSC Adv.* **5** (21), 15954–15961.

Hayyan, M., Abo-Hamad, A., Alsaadi, A. H. & Hashim, M. A. 2015 Functionalization of graphene using deep eutectic solvents. *Nanoscale Res. Lett.* **10** (1), 1–26.

Ji, Z. Y., Shen, X. P., Song, Y. & Zhu, G. X. 2011 *In situ* synthesis of graphene/cobalt nanocomposites and their magnetic properties. *Mater. Sci. Eng. B* **176** (9), 711–715.

Joon, S. L., Hwan, Y. K. & Beum, P. C. 2012 Highly photoactive, low band gap TiO_2 nanoparticles wrapped by graphene. *Adv. Mater.* **24** (8), 1084–1088.

Li, N. W., Zheng, M. B., Chang, X. F., Ji, G. B., Lu, H. L., Xue, L. P., Pan, L. J. & Cao, J. M. 2011 Preparation of magnetic $CoFe_2O_4$-functionalized graphene sheets via a facile hydrothermal method and their adsorption properties. *J. Solid State Chem.* **184** (4), 953–958.

Li, J., Zhang, S. W., Chen, C. L., Zhao, G. X., Yang, X., Li, J. X. & Wang, X. K. 2012 Removal of Cu(II) and fulvic acid by graphene oxide nanosheets decorated with Fe_3O_4 nanoparticles. *ACS Appl. Mater. Interfaces* **4** (9), 4991–5000.

Li, S. M., Wang, B., Liu, J. H. & Yu, M. 2014 In situ one-step synthesis of $CoFe_2O_4$/graphene nanocomposites as high-performance anode for lithium-ion batteries. *Electrochim. Acta* **129**, 33–39.

Liu, M. M., Ru, L. & Wei, C. 2013 Graphene wrapped Cu_2O nanocubes: non enzymatic electrochemical sensors for the detection of glucose and hydrogen peroxide with enhanced stability. *Biosens Bioelectron.* **45** (21), 206–212.

Lu, X., Liu, Y., Bian, X., Chao, D. & Wang, C. 2014 Rapid, microwave-assisted, and one-pot synthesis of magnetic palladium-$CoFe_2O_4$-graphene composite nanosheets and their applications as recyclable catalysts. *Part. Part. Syst. Charact.* **31** (2), 245–251.

Luo, X. G., Liu, S. L., Zhou, J. P. & Zhang, L. N. 2009 *In situ* synthesis of Fe_3O_4/cellulose microspheres with magnetic-induced protein delivery. *J. Mater. Chem.* **19** (21), 3538–3545.

Marcano, D. C., Kosynkin, D. V., Berlin, J. M., Sinitskii, A., Sun, Z., Slesarev, A., Alemany, L. B., Lu, W. & Tour, J. M. 2010 Improved synthesis of graphene oxide. *ACS Nano* **4** (8), 4806–4814.

Qi, T. T., Huang, C. C., Yan, S., Li, X. J. & Pan, S. Y. 2015 Characterization and adsorption properties of magnetite/reduced graphene oxide nanocomposites. *Talanta* **144**, 1116–1124.

Ramesha, G. K., Kumara, A. V., Muralidhara, H. B. & Sampath, S. 2011 Graphene and graphene oxide as effective adsorbents toward anionic and cationic dyes. *J. Colloid Interface Sci.* **361** (1), 270–277.

Sharifi, T., Graciaespino, E., Barzegar, H. R., Jia, X., Nitze, F., Hu, G., Nordblad, P., Tai, C. W. & Wågberg, T. 2013 Formation of nitrogen-doped graphene nanoscrolls by adsorption of magnetic γ-Fe_2O_3 nanoparticles. *Nat. Commun.* **4**, 2319.

Shuang, C. D., Pan, F., Zhou, Q., Li, A., Li, P. H. & Yang, W. B. 2012 Magnetic polyacrylic anion exchange resin: preparation, characterization and adsorption behavior of humic acid. *Ind. Eng. Chem. Res.* **51** (11), 4380–4387.

Sun, H. T., Sun, X., Hu, T., Yu, M. P., Lu, F. Y. & Lian, J. 2014 Graphene-wrapped mesoporous cobalt oxide hollow spheres anode for high-rate and long-life lithium ion batteries. *J. Phys. Chem. C* **118** (5), 2263–2272.

Wan, C. C. & Jian, L. 2015 Synthesis of well-dispersed magnetic $CoFe_2O_4$ nanoparticles in cellulose aerogels via a facile oxidative co-precipitation method. *Carbohydr. Polym.* **134**, 144–150.

Wang, E. W., Lei, S. M., Zhang, S. C., Huang, T. & Zhong, L. L. 2015 Removal of methyl Orange from aqueous solution by mineral-based porous granulated material. *J. Wuhan Uni. Technol.* **30** (1), 185–192.

Wei, H., Yang, W. S., Xi, Q. & Chen, X. 2012 Preparation of Fe_3O_4@graphene oxide core–shell magnetic particles for use in protein adsorption. *Mater. Lett.* **82** (9), 224–226.

Wu, Q. H., Cheng, F., Wang, C. & Zhi, W. 2013 A facile one-pot solvothermal method to produce superparamagnetic graphene-Fe_3O_4 nanocomposite and its application in the removal of dye from aqueous solution. *Colloids Surf. B Biointerfaces* **101** (1), 210–214.

Xie, G. Q., Xi, P. X., Liu, H. Y., Chen, F. Q., Huang, L., Shi, Y. J., Hou, F. P., Zeng, Z. Z. & Shao, C. W. 2012 A facile chemical method to produce superparamagnetic graphene oxide–Fe_3O_4 hybrid composite and its application in the removal of dyes from aqueous solution. *J. Mater. Chem.* **22** (3), 1033–1039.

Xue, W. D., Rui, Z., Xia, D., Xu, F. W., Meng, X. & Wei, K. X. 2014 Graphene-Fe_3O_4 micro-nano scaled hybrid spheres: Synthesis and synergistic electromagnetic effect. *Mater. Res. Bull.* **50** (2), 285–291.

Yang, X. Y., Zhang, X. Y., Ma, Y. F., Huang, Y., Wang, Y. S. & Chen, Y. S. 2009 Superparamagnetic graphene oxide-Fe_3O_4 nanoparticles hybrid for controlled targeted drug carriers. *J. Mater. Chem.* **19** (19), 2710–2714.

Yang, S. B., Feng, X. L., Ivanovici, S. & Müllen, K. 2010 Fabrication of graphene encapsulated oxide nanoparticles: towards high-performance anode materials for lithium storage. *Angew. Chem. Int. Ed.* **49** (45), 8586–8589.

Yao, Y. J., Yang, Z. Z., Zhang, D. W., Peng, W. C., Sun, H. Q. & Wang, S. B. 2012a Magnetic $CoFe_2O_4$–graphene hybrids: facile synthesis, characterization, and catalytic properties. *Ind. Eng. Chem. Res.* **51** (17), 6044–6051.

Yao, Y. J., Miao, S. D., Liu, S. Z., Ma, L. P., Sun, H. Q. & Wang, S. B. 2012b Synthesis, characterization, and adsorption properties of magnetic Fe_3O_4@ graphene nanocomposite. *Integr. Ferroelectr.* **184** (1), 326–332.

Yao, Y. J., Xu, C., Qin, J. C., Wei, F. Y., Rao, M. N. & Wang, S. B. 2013 Synthesis of magnetic cobalt nanoparticles anchored on graphene nanosheets and catalytic decomposition of Orange II. *Ind. Eng. Chem. Res.* **52** (49), 17341–17350.

Zhan, S. H., Zhu, D. D., Ma, S. L., Yu, W. C., Jia, Y. N., Li, Y., Yu, H. B. & Shen, Z. Q. 2015 Highly efficient removal of pathogenic bacteria with magnetic graphene composite. *ACS Appl. Mater. Interfaces* **7** (7), 4290–4298.

Zhang, Y. N. & Nan, Z. D. 2015 Preparation of magnetic $ZnLa_{0.02}Fe_{1.98}O_4$/MWCNTs composites and investigation on its adsorption of methyl orange from aqueous solution. *Mater. Res. Bull.* **66**, 176–185.

Zhang, S., Jiao, Q., Hu, J., Li, J., Zhao, Y., Li, H. & Wu, Q. 2015 Vapor diffusion synthesis of rugby-shaped $CoFe_2O_4$/graphene composites as absorbing materials. *J. Alloys Compd.* **630** (1), 195–201.

Zhao, D. C., Yang, B. & Nan, Z. D. 2015 Synthesis of uniform Co NPs with high saturation magnetization and investigation on removal of methyl orange from aqueous solution by Co/MWCNTs composite. *Mater. Res. Bull.* **68**, 126–132.

First received 9 June 2016; accepted in revised form 27 October 2016. Available online 21 November 2016